

2005

Ab initio study of ferromagnetism in $\text{Ga}_{1-x}\text{Cr}_x\text{N}$ thin films

Qin Wang

Virginia Commonwealth University, QWang3@VCU.edu

Q. Sun

Virginia Commonwealth University

Puru Jena

Virginia Commonwealth University, pjena@vcu.edu

See next page for additional authors

Follow this and additional works at: http://scholarscompass.vcu.edu/phys_pubs

 Part of the [Physics Commons](#)

Wang, Q., Sun, Q., Jena, P. et al. Ab initio study of ferromagnetism in $\text{Ga}_{1-x}\text{Cr}_x\text{N}$ thin films. *Physical Review B*, 72, 045435 (2005). Copyright © 2005 American Physical Society.

Downloaded from

http://scholarscompass.vcu.edu/phys_pubs/91

This Article is brought to you for free and open access by the Dept. of Physics at VCU Scholars Compass. It has been accepted for inclusion in Physics Publications by an authorized administrator of VCU Scholars Compass. For more information, please contact libcompass@vcu.edu.

Authors

Qin Wang, Q. Sun, Puru Jena, J. Z. Yu, R. Note, and Y. Kawazoe

***Ab initio* study of ferromagnetism in $\text{Ga}_{1-x}\text{Cr}_x\text{N}$ thin films**

Q. Wang, Q. Sun, and P. Jena

Physics Department, Virginia Commonwealth University, Richmond, Virginia 23284, USA

J. Z. Yu, R. Note, and Y. Kawazoe

Institute for Materials Research, Tohoku University, Sendai, 980-8577, Japan

(Received 21 December 2004; revised manuscript received 21 March 2005; published 15 July 2005)

Electronic structure and magnetic properties of $\text{Ga}_{1-x}\text{Cr}_x\text{N}$ thin films are studied using the gradient corrected density functional method and a supercell slab model. Calculations are carried out by varying the concentration of doped Cr atoms and the sites they occupy. Cr atoms are found to prefer to reside on the surface sites and cluster around N as Mn atoms do. However, unlike Mn-doped GaN, Cr-doped GaN is found to be ferromagnetic for all concentrations studied. The calculated ferromagnetism is in agreement with recent experimental observations.

DOI: [10.1103/PhysRevB.72.045435](https://doi.org/10.1103/PhysRevB.72.045435)

PACS number(s): 61.46.+w, 36.40.Cg, 75.50.Pp

I. INTRODUCTION

There is considerable current interest in exploiting electron spin in the design and synthesis of novel spin-based electronic materials. The eventual success of these materials for applications in “spintronics” relies on identifying the best candidates for this purpose. Since the theoretical prediction of room-temperature ferromagnetism in Mn-doped GaN,^{1,2} extensive research efforts have been devoted to the study of this system both theoretically and experimentally.³⁻¹⁷ However, the results have been rather confusing. Some experiments reported observation of ferromagnetism in (Ga,Mn)N, while others found it to be antiferromagnetic. It was shown recently that this controversy can be attributed to sample preparation conditions.¹⁸ When Mn atoms are on or near the surface, the contraction in the Mn-Mn bond length results in antiferromagnetic (AFM) coupling. On the other hand, when Mn atoms occupy bulk sites, the coupling becomes ferromagnetic (FM).

Cr is a neighbor to Mn in the Periodic Table, and several groups have recently reported above-room-temperature ferromagnetism for (Ga,Cr)N. Park *et al.*¹⁹ reported room-temperature ferromagnetism ($T_c=280$ K) for bulk single-crystal Cr-doped GaN prepared by the sodium flux growth method. Ferromagnetism with $T_c > 400$ K in (Ga,Cr)N prepared by electron-cyclotron-resonance molecular-beam epitaxy was also reported by Hashimoto *et al.*²⁰ Furthermore, by using epitaxial metalorganic chemical vapor deposition and superconducting quantum interference device magnetometer measurements, Lee *et al.*²¹ found a ferromagneticlike ordering in a Cr-doped GaN sample up to 320 K. Recently, Liu and co-workers²² observed ferromagnetism above 900 K in a Cr-GaN thin film, and showed convincingly that the substitutional Cr atoms are involved in ferromagnetic behavior. Recently theoretical studies of magnetism in bulk (Ga,Cr)N have been carried out,²³ however, no theoretical calculations on Cr-doped GaN thin films are available to our knowledge. The difficulty of thin-film calculation is caused by complicated surface reconstruction that requires the need for large supercells capable of modeling low doping concentrations in experiments.

In this article, we report the first *ab initio* theoretical study

of the electronic and magnetic properties of a Cr-doped GaN thin film. We show that the ferromagnetic phase is energetically the most preferable state, irrespective of the concentration of Cr atoms.

II. COMPUTATIONAL PROCEDURE

We have chosen the $(11\bar{2}0)$ surface of GaN having a wurtzite structure. The thin film was modeled by slabs with different thicknesses. Each slab was separated from the other by a vacuum region of 10 \AA along the $[11\bar{2}0]$ direction. The calculations of total energies and forces, and optimizations of geometry were carried out using the density functional theory (DFT) and PW91 functional²⁴ for the generalized gradient approximation (GGA) for exchange and correlation potential. A plane-wave basis set and the projector augmented wave (PAW) potentials²⁵ for Ga, Cr, and N, as implemented in the Vienna *Ab initio* Simulation Package (VASP),²⁶ were employed. The energy cutoff was set at 300 eV, and the convergence in energy and force were 10^{-4} eV and 10^{-3} eV/ \AA , respectively. The accuracy of our computational procedure has been established in our earlier work,¹⁸ where we calculated the main geometrical parameters and cohesive energies of bulk GaN by carrying out full geometrical relaxation with different supercell sizes and compared the results with experiments.

III. RESULTS AND DISCUSSIONS

The properties of Cr-doped GaN thin films have been studied in succeeding steps. We begin this work by first discussing the properties of an undoped GaN $(11\bar{2}0)$ thin film. The thin film was modeled by a nine-layer (1×2) GaN $(11\bar{2}0)$ slab that consists of 36 Ga and 36 N atoms, as shown in Fig. 1. The central three layers of the slab were held at their bulk configuration while the three layers on either side of the slab were allowed to relax without any symmetry constraint. To preserve the symmetry, the top and bottom layers of the slab have been taken to be identical in all the following calculations. The surface reconstruction was carried out

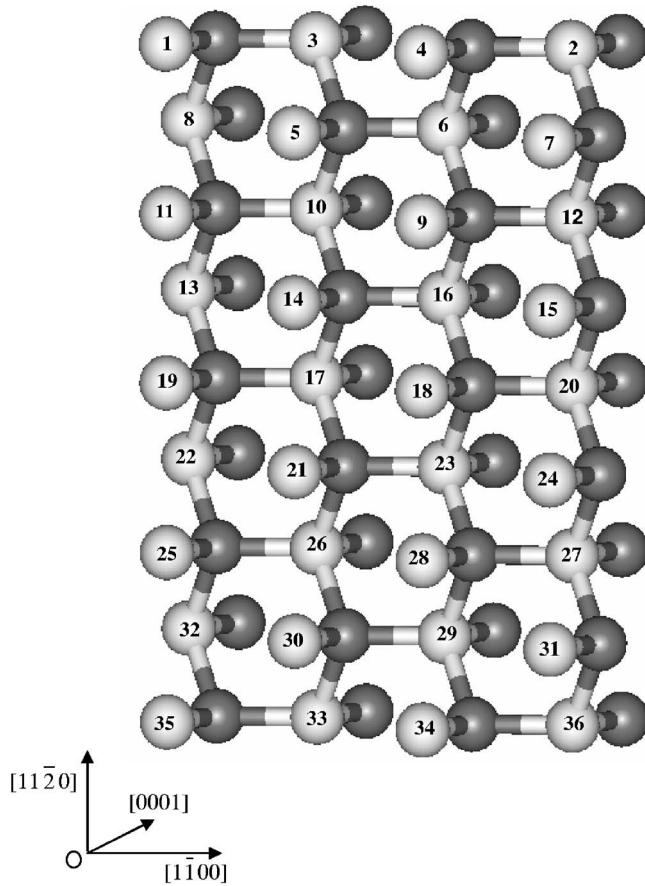


FIG. 1. Schematic representation of a nine-layer slab model for the wurtzite GaN $(11\bar{2}0)$ surface, which consists of 36 Ga and 36 N atoms. The lighter and numbered spheres represent Ga, and the darker spheres represent N.

by full geometry optimization of the slab. The K -point convergence was achieved with a $(6 \times 4 \times 1)$ Monkhorst-Pack grid²⁷ for the geometry optimization and $(8 \times 6 \times 2)$ for the final calculation, corresponding to 12 and 24 irreducible K points in the first Brillouin zone, respectively. The total energy of the relaxed slab is 3.176 eV lower than the unrelaxed one, corresponding to an energy gain of 0.132 eV/Ga-N dimer. The vertical buckling Δ_{\perp} of the Ga-N dimer on the surface atomic layer is +0.234 Å, while that on the subsurface layer is -0.04 Å. The bond length of Ga-N on the surface layer is 1.895 Å along the $[1\bar{1}00]$ direction and 1.874 Å along the $[0001]$ direction, which are contracted by -1.76% and -5.35%, as compared with the bulk, respectively. It is found that the relaxation occurs mainly in the surface layer, while the relaxations of the atoms in the subsurface layer and the third layer are an order of magnitude smaller than that in the surface layer. The total density of states (DOS) for the slab is plotted in Fig. 2(a). From the DOS, we can see that the Fermi level is located in the gap region, confirming that GaN is a semiconductor. The DOS curves for spin-up and spin-down states are totally symmetric, therefore there is no net magnetic moment in this thin-film system. In addition, no surface states are present in the band gap.

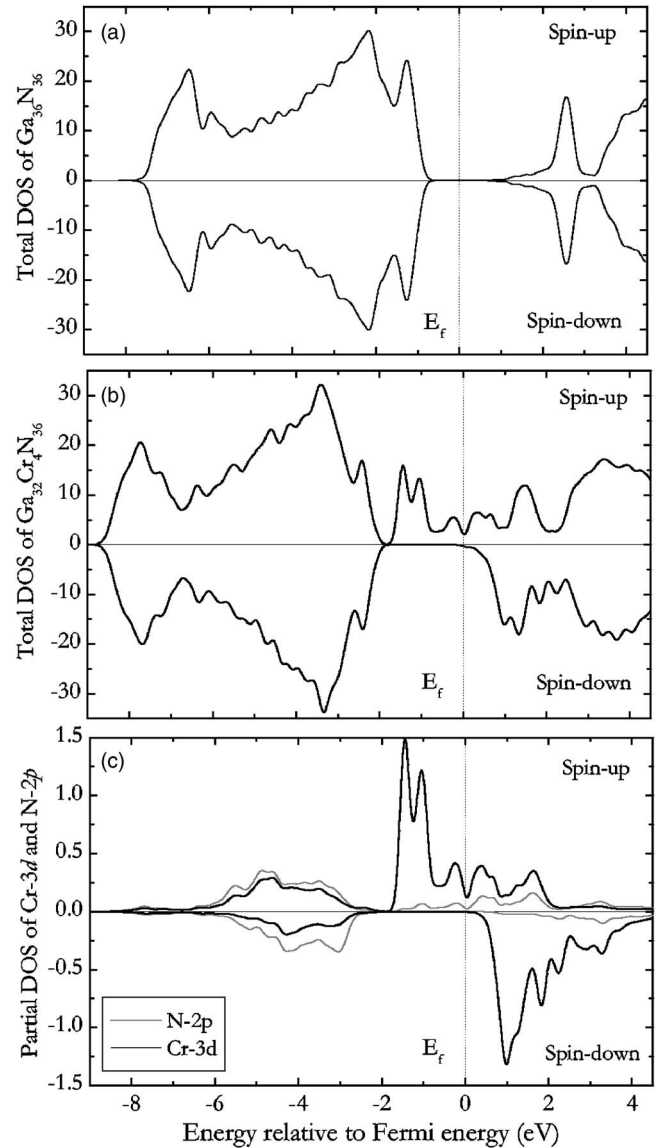


FIG. 2. (a) Total DOS of $\text{Ga}_{36}\text{N}_{36}$ corresponding to an undoped wurtzite $(11\bar{2}0)$ GaN surface. (b) Total DOS of the $\text{Ga}_{32}\text{Cr}_4\text{N}_{36}$ slab, corresponding to a Cr-doped GaN thin film with 11% Cr concentration. (c) Partial DOS of Cr-3d and N-2p at neighboring sites in $\text{Ga}_{32}\text{Cr}_4\text{N}_{36}$.

To study the site preference of a Cr atom, we first replaced a *single* Ga atom with Cr in the top layer of the slab. To preserve symmetry, a Cr atom was also substituted at the corresponding Ga site in the bottom layer of the slab. This substitution leads to a supercell consisting of $\text{Ga}_{34}\text{Cr}_2\text{N}_{36}$ and amounts to a 5.6% Cr concentration. We have also checked the possibility that Cr may prefer a subsurface site. This is achieved by replacing a Ga atom in the subsurface and the third layer on either side of the slab. Specifically, the Ga atoms at site Nos. 3, 6, and 10 in the top side and at site Nos. 33, 29, and 26 in the bottom side of the slab have been replaced with Cr atoms, respectively. The distance between the two Cr atoms in either side of the slab for these three configurations is 12.684, 9.513, and 6.342 Å, respectively. This is quite large and thus the interaction between these two

TABLE I. Optimized Cr-Cr distance (in Å), relative energy $\Delta\varepsilon$ (in eV) calculated with respect to the ground state (configuration I), energy difference between AFM and FM states $\Delta E = E_{\text{AFM}} - E_{\text{FM}}$ (in eV), and moments (in μ_B) at Cr and its nearest-neighbor N and Ga atoms for each configuration.

Configuration (Cr sites)	(Cr-Cr) distance	$\Delta\varepsilon$	ΔE	Local moments				
				μ^{total}	μ^s	μ^p	μ^d	
I. (1, 3/35, 33)	3.064	0	0.512	Cr	2.742	0.050	0.018	2.674
				N	-0.157	-0.014	-0.142	
				Ga	0.026	0.016	0.007	0.003
II.(3, 4/33, 34)	4.515	1.034	-0.061	Cr	2.602	0.050	0.006	2.551
				N	-0.055	-0.003	-0.054	
				Ga	0.036	0.018	0.017	0.002
III.(2, 3/33, 36)	5.494	1.059	-0.032	Cr	2.619	0.044	0.005	2.565
				N	-0.052	-0.003	-0.051	
				Ga	0.037	0.018	0.018	0.001
IV.(3, 6/33, 29)	3.14	2.15	-0.17	Cr	2.534	0.012	0.007	2.485
				N	-0.057	-0.004	-0.054	
				Ga	0.033	0.021	0.019	0.001
V. (5, 6/29, 30)	3.077	3.014	-0.204	Cr	1.988	0.022	0.013	1.952
				N	0.008	0.001	0.008	
				Ga	0.034	0.022	0.008	0.003

Cr atoms can be neglected. We found that the Cr atom prefers to reside on the surface layer, which is 1.55 and 1.91 eV lower in energy than that of the Cr located in the subsurface and third layer, respectively. This is similar to the results obtained in the Mn-doped GaN (11 $\bar{2}$ 0) surface.¹⁸

Next, using the above slab model, we studied the coupling between Cr atoms by replacing two Ga atoms with Cr on both the top and bottom sides of the slab. This replacement generated a Ga₃₂Cr₄N₃₆ supercell with 11% Cr doping. Since it is *a priori* not clear how these Cr atoms are distributed relatively, we have studied five possible configurations in which the two Cr atoms replace Ga at the nearest, second-nearest, and third-nearest sites in the surface layer, the nearest sites in subsurface layer, and one Ga in surface layer and another one in the subsurface layer. The results are summarized in Table I. In the first column, we specified the Ga atoms that were replaced by Cr as shown in Fig. 1. For instance, configuration I (1, 3/35, 33) corresponds to replacing Ga atoms at site Nos. 1 and 3 on the top side of the slab, and symmetrically replacing Ga at site Nos. 35 and 33 on the bottom side. Total energies corresponding to both FM and AFM spin alignments were calculated to determine the preferred magnetic ground state for all these configurations. The magnetic moments at each Cr site were calculated self-consistently. The self-consistent procedure was started by initially assigning a magnetic moment of 5 μ_B at each Cr site for both FM and AFM configurations. The optimized Cr-Cr distance and the relative energy $\Delta\varepsilon$, which is measured with respect to the ground-state energy for each configuration, are listed in the second and third columns of Table I. It is found that configuration I with FM coupling has the lowest total energy than all others, and the energy increases remarkably when Cr atoms occupy the interior sites of the thin film. The energy difference ΔE between AFM and FM states (ΔE

$= E_{\text{AFM}} - E_{\text{FM}}$) and the calculated local magnetic moments on Cr atom and its nearest anion N and cation Ga for each of five configurations are given in the fourth and fifth columns of Table I. For the most stable configuration I, the FM state is 0.512 eV lower in energy than the AFM state, where the two Cr atoms prefer to occupy the surface layer, and cluster around N atoms. The Cr-N bond length in the surface layer is 1.815 and 1.857 Å along [1 $\bar{1}$ 00] and [0001], respectively. This corresponds to a contraction of -4.22% and -0.91% as compared with the undoped GaN surface, respectively. It is obvious that the energy different ΔE becomes smaller and smaller as the Cr-Cr distance increases, although the FM state is not always lower in energy for all the other four configurations. In the ground state, each Cr atom carries 2.74 μ_B , which is close to the experimental value of 3.0 μ_B for the ideal substitutional case.²² This suggests that the Cr impurity doped in GaN has a magnetic configuration of $3d^3$. The neighboring N atom of Cr is polarized antiferromagnetically with a magnetic moment of 0.157 μ_B , which mainly comes from the N-2p orbital (0.142 μ_B). The total DOS and the partial Cr-3d and N-2p DOS are shown in Figs. 2(b) and 2(c), respectively. We note that the system is half metallic with Cr-3d dominating the DOS at the Fermi energy. Meanwhile, there is a noticeable overlap between Cr-3d and N-2p states. In particular, the majority N-2p orbitals are more hybridized with Cr-3d orbitals than the minority states. This results in opposite magnetic moments of N atoms, similar to what happened in CrN bulk²⁸ and Cr₂N and Cr₂O clusters.²⁹⁻³¹ The charge density distribution plotted in Fig. 3(a) is consistent with the above picture. It shows that there is a strong interaction between Cr and the nearing N atoms.

To study the change of magnetic coupling between Cr atoms with Cr concentration, we made additional calculations by changing the thickness along the [11 $\bar{2}$ 0] and [0001]

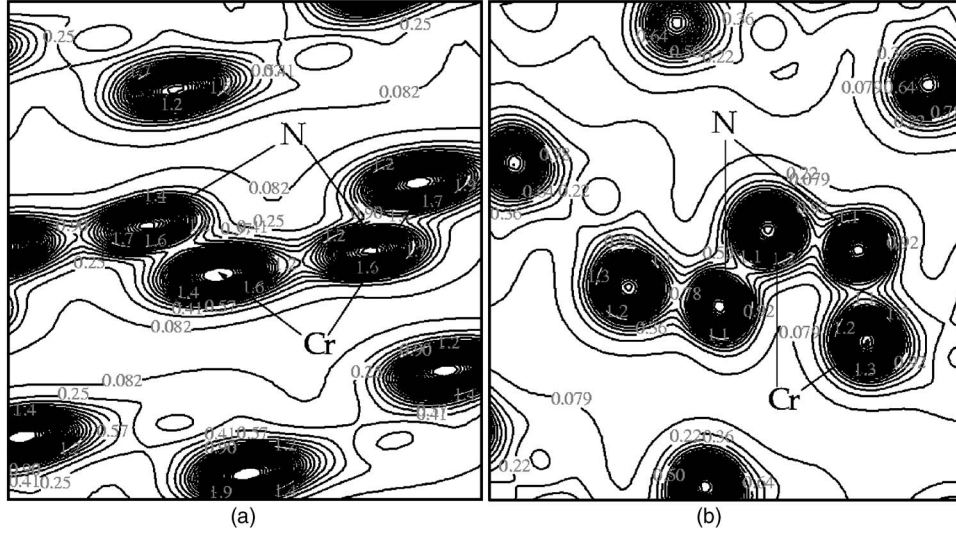


FIG. 3. Charge density distribution in (a) $\text{Ga}_{32}\text{Cr}_4\text{N}_{36}$ and (b) $\text{Ga}_{52}\text{Cr}_4\text{N}_{56}$ supercells in the plane containing Cr and neighboring N atoms.

directions. We first increased the thickness of the slab along the $[11\bar{2}0]$ direction to 11 layers based on the above (1×2) nine-layer model, which contains a total of 88 atoms ($\text{Ga}_{44}\text{N}_{44}$). We fixed the atoms in the central five layers at the bulk position, and fully relaxed both the top and bottom three layers of the slab. We still used Monkhorst-Pack K -point mesh of $6 \times 4 \times 1$ for the geometry optimization and $8 \times 6 \times 2$ for the final calculation. The surface reconstruction and simulation of the Cr-doped GaN thin film have been carried out by following a similar procedure as discussed above. The energy gain due to the relaxation was found to be 0.131 eV/Ga-N dimer. The Ga-N bond lengths in the surface and subsurface layers were found to converge to the nine-layer slab. The substitution of two Ga atoms with Cr on either side of the slab corresponds to a 9% Cr doping concentration. By searching all the possible Ga sites that Cr atoms can replace, it was found that the Cr atoms again prefer to reside on the surface layer and cluster around N atoms. The FM state is found to be 0.504 eV lower in energy than the AFM state. Each Cr atom carries a magnetic moment of $2.74 \mu_B$, and the moments located on Cr- $3d$, Cr- $4s$, and Cr- $4p$ are essentially the same as the values we obtained from the nine-layer slab model. We also performed the calculation for the (1×2) seven-layer slab, which consists of 28 Ga atoms and 28 N atoms. The FM state is once again found to be lower in energy than that of AFM by 0.528 eV, and the

Cr atoms prefer to occupy the surface layer sites and cluster around the N atoms. The local magnetic moments distributed on the Cr and neighboring N are given in Table II. It is clear that the energy and magnetic moments are close to the values obtained for the nine-layer slab.

There is an important point we need to clarify in the above seven- to 11-layer slab models. When a (1×2) surface unit cell is used for constructing the slabs, the Cr atoms on the surface form continuous chains along the $[0001]$ direction. The question is whether the coupling is still ferromagnetic when Cr atoms do not form continuous chains. To check this point, we used a seven-layer (2×2) slab model containing 56 Ga atoms and 56 N atoms. The central three layers of this slab were fixed at a bulk crystalline position, while both the top and bottom two layers were relaxed without any symmetry constraint. The geometry of the supercell was optimized fully by using $(5 \times 5 \times 1)$ Monkhorst-Pack K -point mesh.²⁷ For the final calculation of total energy and magnetic moments, we used $(6 \times 6 \times 2)$ K -point mesh. When two Cr atoms are substitutionally doped at Ga sites on either side of the slab, a $\text{Ga}_{52}\text{Cr}_4\text{N}_{56}$ supercell with a 7% Cr concentration is generated. There are many more possible Ga sites for Cr atoms to replace, since there are twice as many Ga-N dimers in each layer of this slab. We did extensive search by replacing Ga with Cr at different sites in the surface layer and/or subsurface layer. We found that Cr atoms continue to prefer to reside in the surface layer and cluster

TABLE II. Cr doping concentration, slab size, corresponding supercell, energy difference (ΔE) between AFM and FM states per Cr atom (in eV/Cr), and local magnetic moments (in μ_B) located on Cr (μ_{Cr}) and N (μ_{N}).

Concentration	Slab size	Supercell	ΔE	Coupling	μ_{Cr}	μ_{N}
0.07	Seven-layer (2×2)	$\text{Ga}_{52}\text{Cr}_4\text{N}_{56}$	0.121	FM	2.626	-0.11
0.09	11-layer (1×2)	$\text{Ga}_{40}\text{Cr}_4\text{N}_{44}$	0.128	FM	2.742	-0.15
0.11	Nine-layer (1×2)	$\text{Ga}_{32}\text{Cr}_4\text{N}_{36}$	0.126	FM	2.742	-0.15
0.143	Seven-layer (1×2)	$\text{Ga}_{24}\text{Cr}_4\text{N}_{28}$	0.132	FM	2.742	-0.16

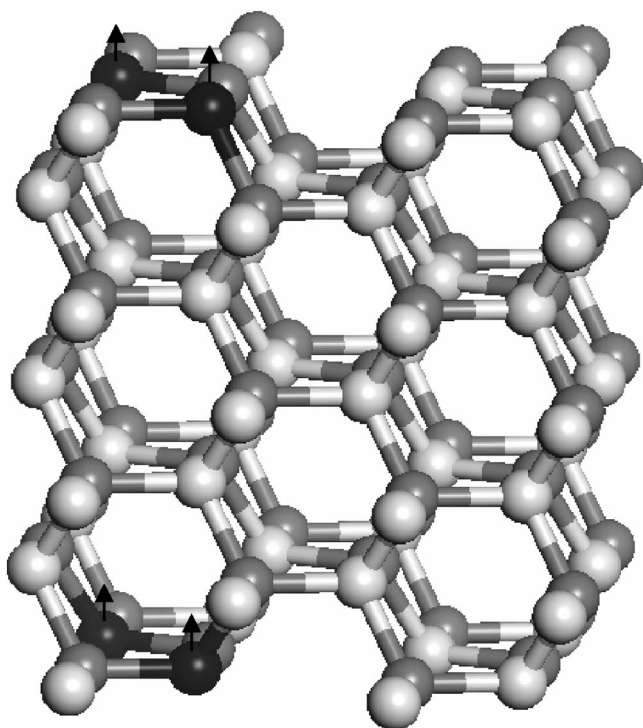


FIG. 4. Schematic representation of a seven-layer $\text{Ga}_{52}\text{Cr}_4\text{N}_{56}$ ($11\bar{2}0$) slab, corresponding to 7% Cr doping concentration.

around the N atom. Figure 4 shows the most stable configuration of the $\text{Ga}_{52}\text{Cr}_4\text{N}_{56}$ slab. The Cr-N bond length was found to be 1.833 and 1.859 Å along the $[1\bar{1}00]$ and $[0001]$ directions, respectively. The energy difference between the AFM and FM states is 0.121 eV/Cr atom with the FM state lying lower in energy. The Cr atom carries a magnetic moment of $2.626 \mu_B$, contributed mainly from $3d(2.574 \mu_B)$ and $4s(0.049 \mu_B)$ orbitals of Cr. The partial DOS of the Cr atom are shown in Fig. 5(b), which can be compared with the total DOS given in Fig. 5(a). The N atoms forming the nearest neighbor to Cr are polarized antiferromagnetically and carry a moment of $0.11 \mu_B$ mainly arising from N-2p orbitals. The charge density distribution in the plane of Cr-N-Cr of the surface layer is given in Fig. 3(b). This differs from the results in Fig. 3(a) when Cr atoms form a continuous line.

To further understand the mechanism involved in the ferromagnetic coupling between the two Cr atoms doped in GaN, we revisit the DOS shown in Figs. 2 and 5. Note that there are three common features: (1) All DOS show a half-metallic character. (2) Cr-3d orbitals hybridize with N-2p orbitals. In addition, doping Cr in GaN induces some changes in the N-2p DOS, as found in the recent experiment.³² (3) The impurity states, which originate from the hybridization between Cr-3d and N-2p, appear in the band region. These features are very similar to what has been found in bulk Cr-doped GaN,³²⁻³⁴ where the displayed ferromagnetism was driven by double-exchange interactions.³⁵ Therefore, we conclude that the double-exchange mechanism is also responsible for ferromagnetism observed in Cr-doped GaN thin films.

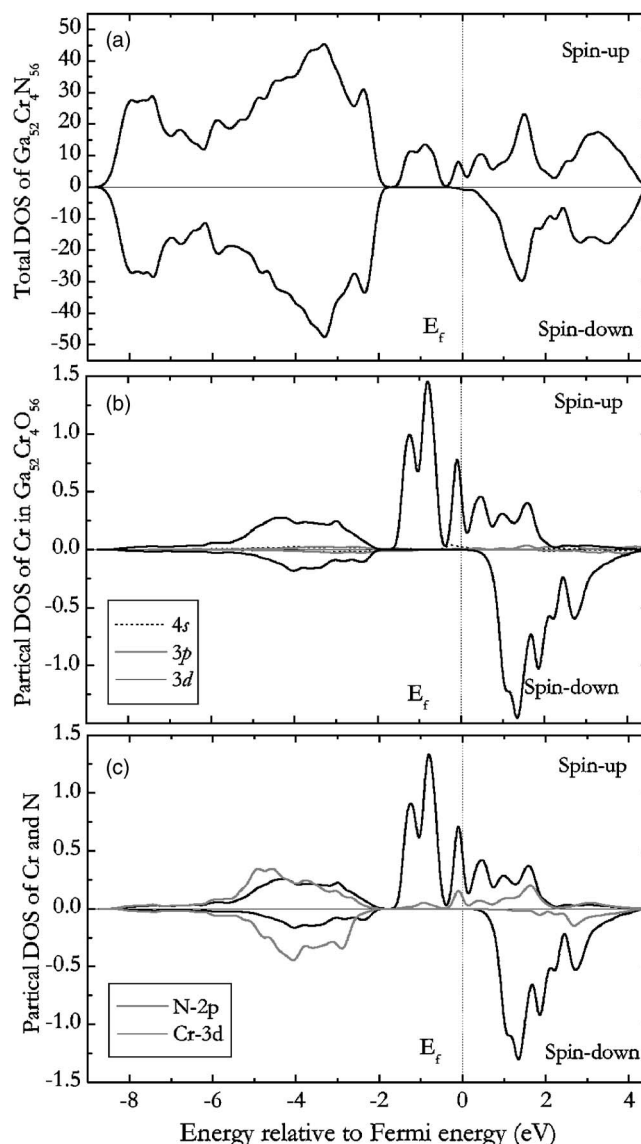


FIG. 5. (a) Total DOS, (b) partial DOS of Cr, and (c) partial DOS of Cr-3d and neighboring N-2p for the $\text{Ga}_{52}\text{Cr}_4\text{N}_{56}$ slab shown in Fig. 4.

IV. SUMMARY

We have studied the magnetic properties of a Cr-doped GaN thin film using the density functional theory and generalized gradient approximation for exchange and correlation potential. We show that Cr atoms cluster around N on the surface layer of the thin film and, in agreement with recent experiments, ferromagnetic coupling is energetically more preferable than antiferromagnetic coupling. We also find the preferred coupling between Cr atoms to be ferromagnetic irrespective of Cr concentration and whether Cr atoms remain on the surface or in the bulk. The ferromagnetic coupling is driven by a double-exchange mechanism. These results are in contrast to Mn-doped GaN, where the Mn atoms couple antiferromagnetically on the surface, but ferromagnetically in the bulk. The ferromagnetism exhibited in bulk and in the thin film makes Cr-doped GaN a promising candidate for applications in spintronics.

ACKNOWLEDGMENTS

The work was supported in part by a grant from the Office of Naval Research. The authors thank the crew of the Center

for Computational Materials Science, the Institute for Materials Research, Tohoku University (Japan), for their continuous support of the HITACHI SR8000 supercomputing facility.

-
- ¹H. Ohno, *Science* **281**, 951 (1998).
²T. Dietl, H. Ohno, F. Matsukura, J. Cibert, and D. Ferrant, *Science* **287**, 1019 (2000).
³M. L. Reed, M. K. Ritums, H. H. Stadelmaier, M. J. Reed, C. A. Parker, S. M. Bedai, and N. A. El-Masry, *Mater. Lett.* **51**, 500 (2001).
⁴M. L. Reed, N. A. El-Masry, H. H. Stadelmaier, M. K. Ritums, M. J. Reed, C. A. Parker, J. C. Roberts, and S. M. Bedair, *Appl. Phys. Lett.* **79**, 3473 (2001).
⁵S. Sonoda, S. Shimizu, T. Sasaki, Y. Yamamoto, and H. Hori, *J. Cryst. Growth* **237-239**, 1358 (2002).
⁶T. Sasaki, S. Sonoda, Y. Yamamoto, K. Suga, S. Shimizu, K. Kindo, and H. Hori, *J. Appl. Phys.* **91**, 7911 (2002).
⁷G. T. Thaler, M. E. Overberg, B. Gila, R. Frazier, C. R. Abernathy, S. J. Pearton, J. S. Lee, S. Y. Lee, Y. D. Park, Z. G. Khim, J. Kim, and F. Ren, *Appl. Phys. Lett.* **80**, 3964 (2002).
⁸J. M. Lee, K. I. Lee, J. Y. Chang, M. H. Ham, K. S. Huh, J. M. Myoung, W. J. Hwang, M. W. Shin, S. H. Han, H. J. Kim, and W. Y. Lee, *Microelectron. Eng.* **69**, 283 (2003).
⁹P. P. Chen, H. Makino, J. J. Kim and T. Yao, *J. Cryst. Growth* **251**, 331 (2003).
¹⁰S. S. A. Seo, M. W. Kim, Y. S. Lee, T. W. Noh, Y. D. Park, G. T. Thaler, M. E. Overberg, C. R. Abernathy, and S. J. Pearton, *Appl. Phys. Lett.* **82**, 4749 (2003).
¹¹Y. Shon, Y. H. Kwon, Sh. U. Yuldashev, Y. S. Park, D. J. Fu, D. Y. Kim, H. S. Kim, and T. W. Kang, *J. Appl. Phys.* **93**, 1546 (2003).
¹²T. Kondo, S. Kuwabara, H. Owa, and H. Munekata, *J. Cryst. Growth* **237-239**, 1353 (2002).
¹³S. Dhar, O. Brandt, A. Trampert, L. Däweritz, K. J. Friedland, K. H. Ploog, J. Keller, B. Beschoten, and G. Güntherodt, *Appl. Phys. Lett.* **82**, 2077 (2003).
¹⁴S. Dhar, O. Brandt, A. Trampert, K. J. Friedland, Y. J. Sun, and K. H. Ploog, *Phys. Rev. B* **67**, 165205 (2003).
¹⁵K. H. Ploog, S. Dhar, and A. Trampert, *J. Vac. Sci. Technol. B* **21**, 1756 (2003).
¹⁶M. Zajac, J. Gosk, M. Kamiska, A. Twardowski, T. Szyszko, and S. Podsiado, *Appl. Phys. Lett.* **79**, 2432 (2001).
¹⁷K. Ando, *Appl. Phys. Lett.* **82**, 100 (2003).
¹⁸Q. Wang, Q. Sun, P. Jena, and Y. Kawazoe, *Phys. Rev. Lett.* **93**, 155501 (2004).
¹⁹S. E. Park, H.-J. Lee, Y. C. Cho, S.-Y. Jeong, C. R. Cho, and S. Cho, *Appl. Phys. Lett.* **80**, 4187 (2002).
²⁰M. Hashimoto, Y.-K. Zhou, M. Kanamura, and H. Asahi, *Solid State Commun.* **122**, 37 (2002).
²¹J. S. Lee, J. D. Lim, Z. G. Khim, Y. D. Park, S. J. Pearton, and S. N. G. Chu, *J. Appl. Phys.* **93**, 4512 (2003).
²²H. X. Liu, Stephen Y. Wu, R. K. Singh, Lin Gu, David J. Smith, N. Newman, N. R. Dilley, L. Montes, and M. B. Simmonds, *Appl. Phys. Lett.* **85**, 4076 (2004).
²³K. Sato and H. K. Yoshida, *Semicond. Sci. Technol.* **17**, 367 (2002).
²⁴Y. Wang and J. P. Perdew, *Phys. Rev. B* **44**, 13298 (1991).
²⁵P. E. Bloechl, *Phys. Rev. B* **50**, 17953 (1994).
²⁶G. Kresse and J. Heffner, *Phys. Rev. B* **54**, 11169 (1996).
²⁷H. J. Monkhorst and J. D. Pack, *Phys. Rev. B* **13**, 5188 (1976).
²⁸I. Galanakis and P. Mavropoulos, *Phys. Rev. B* **67**, 104417 (2003).
²⁹Q. Wang, Q. Sun, B. K. Rao, P. Jena, and Y. Kawazoe, *J. Chem. Phys.* **119**, 7124 (2003).
³⁰K. Tono, A. Terasaki, T. Ohta, and T. Kondow, *Phys. Rev. Lett.* **90**, 133402 (2003).
³¹K. Tono, A. Terasaki, T. Ohta, and T. Kondow, *J. Chem. Phys.* **119**, 11221 (2003).
³²T. Takeuchi, Y. Harada, T. Tokushima, M. Taguchi, Y. Takata, A. Chainani, J. J. Kim, H. Makino, T. Yao, T. Yamamoto, T. Tsukamoto, S. Shin, and K. Kobayashi, *Phys. Rev. B* **70**, 245323 (2004).
³³K. Sata, P. H. Dederichs, H. Katayama-Yoshida, and J. Kudrnovsky, *Physica B* **340-342**, 863 (2003).
³⁴K. Sato, P. H. Dederichs, and H. Katayama-Yoshida, *Europhys. Lett.* **61**, 403 (2003).
³⁵H. Akai, *Phys. Rev. Lett.* **81**, 3002 (1998).